JOURNAL OF GUIDANCE, CONTROL, AND DYNAMICS
Vol. 29, No. 3, May–June 2006

Feasible Flight Paths for Cooperative Generation of a Phantom Radar Track

Keith B. Purvis*
University of California, Santa Barbara, California 93106-5070
Phillip R. Chandler†
U.S. Air Force Research Laboratory, Wright–Patterson Air Force Base, Ohio 45433-7531
and
Meir Pachter‡
Air Force Institute of Technology, Wright–Patterson Air Force Base, Ohio 45433-7765

Electronic attack on air defense radar networks by electronic combat air vehicles (ECAVs) is considered. The scope of the attack is the creation of a coherent phantom track in two dimensions—range and azimuth—by a team of cooperatively controlled ECAVs, each capable of intercepting and sending delayed returns of radar pulses. It is first shown that assuming constant speeds for the phantom track and ECAVs severely restricts where the ECAVs can fly. Accordingly, general dynamic and spatial limitations on an ECAV are developed given ranges on the ECAV speed, phantom track speed, and ECAV region of antenna operation; six dynamical systems are also constructed for simulating feasible ECAV trajectories to test the analytical limitations. This theory is applied to construct detailed flyable ranges for an ECAV generating a straight and a circular phantom track, separately. Based on distilling the results, generalized bounds are presented—independent of the phantom track type—for the initial conditions and time-dependent flyable ranges of a team of ECAVs. These bounds are then used with coordination functions to informally solve an illustrative decentralized cooperative control problem in which the ECAV team seeks an optimal straight phantom track to minimize their bounds-dependent aggregate cost.

Nomenclature

a	=	x coordinate of radar with reference to center of circular phantom track
a_E	=	electronic combat air vehicle (ECAV) acceleration—magnitude of time derivative of velocity
B	=	space where placement of a phantom track is possible for all radar/ECAV pairs
b	=	y coordinate of radar with reference to center of circular phantom track
C	=	cone-shaped set of points on which ECAV's antennas can see its radar
c	=	speed of light
D	=	disk-shaped set of points on which radar can operate and see targets
h_E	=	ECAV heading angle
n	=	number of radars participating in a network
p	=	location of radar in x and y coordinates
R	=	phantom target range from radar
$R_{\max}$	=	maximum operational range of radar
r	=	ECAV range from radar
s	=	switching function
$\mathcal{T}_B$	=	set of all phantom track functions possible for ECAV team to generate
t	=	time
t_s	=	switching time
X	=	x coordinate of phantom track
Y	=	y coordinate of phantom track
α	=	ratio of phantom target speed to nominal mean ECAV speed
β	=	bearing from center of circular phantom track to radar
θ	=	bearing from radar to ECAV and phantom target
ρ	=	radius of circular phantom track
υ	=	speed of ECAV or phantom target
Φ	=	absolute heading angle of straight phantom track—independent of all radar locations
ϕ	=	course angle of ECAV or phantom target—relative to current line of sight (LOS)
χ	=	angle between current LOS and line from center of circular phantom track to radar
ψ	=	angle between initial LOS and straight phantom track

Subscripts

c	=	variable set constant
E	=	pertaining to ECAV
f	=	value at the final time
i	=	index number for radar/ECAV pair
m	=	nominal mean
psmax	=	pseudomaximum
psmin	=	pseudominimum
T	=	pertaining to phantom target
0	=	value at the initial time

Superscripts

A	=	solution corresponding to ECAV system A
f	=	solved backward in time using final values
0	=	solved forward in time using initial values

Presented as Paper 2004-5335 at the AIAA Guidance, Navigation, and Control Conference, Providence, RI, 16–19 August 2004; received 28 January 2005; revision received 16 August 2005; accepted for publication 4 August 2005.

*Graduate Student Researcher, Department of Mechanical and Environmental Engineering, Engineering II Building Room 2355. Student Member AIAA.

†Senior Control Systems Engineer, AFRL/VACA, 2210 8th Street. Senior Member AIAA.

‡Professor, Department of Electrical and Computer Engineering, 2950 P Street, Building 640 Room 224. Associate Fellow AIAA.

I. Introduction

THIS work focuses on using unmanned electronic combat air vehicles (ECAVs) to cooperatively deceive an enemy radar network by generating a coherent phantom track, that is, causing the network to detect and track the motion of an air vehicle that does not actually exist; how the phantom track is generated will be explained in the next section. This tactic, referred to as *technique deception*, is actually one of many (noise deception, jamming, directed energy, etc.) that could be employed for electronic attack (EA) in an electronic warfare (EW) scenario.[1,2] Developing an effective EA capability is of interest because it is challenging scientifically, and it has been identified as one of the top 10 military goals for unmanned aviation.[3] Strategically, this EA tactic might be used to divert attention away from another area in the battlefield or to impose a virtual threat on the opposition. Creating a false target track that is 1) coupled to its creator air vehicle's free flight path and 2) for a single radar is not a new concept.[4] The novelty of the technique deception problem investigated here is that now the track 1) can be freely/firstly chosen and 2) must appear spatially and temporally consistent to a radar network. The important question, then—and what this research concentrates on—is how an ECAV team's trajectories are constrained for such a track.

For practical purposes, an ECAV is regarded as relatively inexpensive and small enough to be undetected by a radar at realistic ranges; furthermore, it can accurately obtain its position, synchronize its clock to a standard, and communicate with other ECAVs. A radar network is defined as a geometric arrangement (possibly changing with time) of two or more radars, which are able to communicate; thus, multiple radars can track and correlate the same target. Generating a viable coherent phantom track requires a specified set of the networked radars to detect a consistent position (range and azimuth) and range rate for the phantom target as it moves along. The methods considered herein to accomplish this task of technique deception are restricted to range-delay techniques applied through the radar main lobe or beamwidth. Clearly, for a team of ECAVs—generally one per radar—attempting to deceive a radar network in such a way, the flyable trajectories of each individual ECAV are confined to some exclusive range. For additional background reading, see Ref. 5 on radar basics and Refs. 2 and 6 on EA and EW.

A broad and descriptive introduction to the technique deception problem can be found in Refs. 7 and 8, which do include some earlier simplified results taken from this work on ECAV flyable regions. A preliminary version of this work was presented at the 2004 AIAA GNC Conference.[9] References 7 and 8 mathematically describe the dynamics of a constant-speed ECAV given a straight or simple circular phantom track (radar at circle center) with constant speed. This work begins by showing through simulation that assuming an ECAV has constant speed places unreasonable limits on its feasible initial conditions and trajectories given a straight constant-speed phantom track. In response, a more general theory for modeling ECAV dynamics mathematically and developing bounds for ECAV trajectories is contributed, which allows for ranges on the ECAV and phantom track speeds as well as limitations on the ECAV antenna operation regions. This theory is used to work out the flyable ranges for an ECAV given a straight or general circular phantom track. Note that extensive ECAV trajectory simulations were used to test these flyable ranges, but only the trajectory planning algorithms used for simulation are presented in this paper. Generalized mathematical bounds for a team of ECAVs—independent of whether the phantom track is straight or circular—are provided, and a decentralized cooperative control problem is constructed as an example that relies on these bounds. Developing effective cooperative control strategies for EA, among other tactical missions, is itself a subject of interest and must address the principal challenges of coupled tasks, partial information restrictions, and communication delays[10].

II. Explanation of the Deception Problem

Assuming that an ECAV knows the maximum operational range $R_{\max}$ and location of a radar with pulse-to-pulse agility or discrimination, the ECAV can intercept and send delayed returns of the radar's transmitted pulses so that the radar sees a phantom target at a range beyond the ECAV but closer than $R_{\max}$. The capability of digitally storing, altering, and retransmitting encoded pulses so that they correspond to a desired range and range rate is formally known as digital radio frequency memory (DRFM), but will normally be referred to here simply as range delay because it is assumed that DRFM will be used to accomplish this task (see Refs. 4 and 5 for more information). Using only range delay for technique deception requires that the ECAV be in the radar main lobe or line of sight (LOS); of course, the phantom target will also be on the LOS from the radar to the ECAV. Thus, the phantom target's track is a function of the ECAV's range delay and bearing from the radar over time. If the radar operates at a pulse repetition frequency (PRF) where pulse-delay ranging is performed, then accurately delaying the radar's pulses is crucial. If the radar operates at higher PRFs in track mode, then range information is still important, but the ECAV can focus on sending returns with accurate Doppler frequencies or range rates for the phantom target.[5] Keep in mind that a phantom track flying roughly perpendicular to a radar will not produce significant Doppler frequencies and might even get filtered out or ignored.

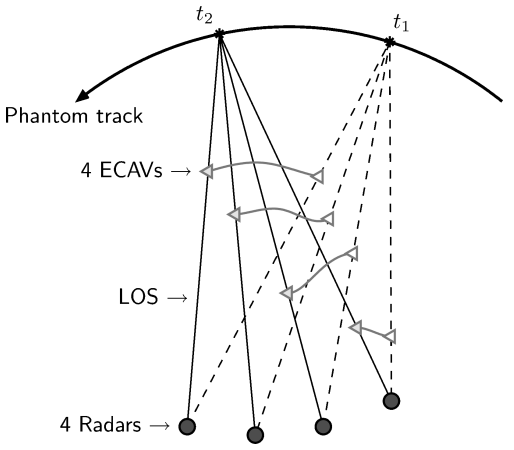

Fig. 1 Main-lobe technique deception of a radar network by creation of a phantom track.

Figure 1 illustrates how four ECAVs could cooperatively create a single phantom track to deceive a network of four radars by using range-delay techniques. For this example, where all four of the radars share track files, unless all radars see the same phantom track, the track is dismissed as spurious. To study only the critical challenges of the proposed deception concept, a planar or constant-elevation scenario is focused on. The proposed concept is also valid in three dimensions, but this case is not much more interesting than the two dimensional case because it adds few additional constraints. In general, the phantom flies at a constant altitude, and any minor descents can be easily handled and decoupled by the ECAVs.

The key "inverse problem" is to determine the allowable trajectories for the ECAVs given a time-dependent phantom track. Observing Fig. 1, each ECAV behaves much like a bead on a string that is rotating at some variable rate; the ECAV can slide up and down freely but must rotate with the LOS from the radar to the phantom track. If its speed, heading, or another variable is constrained in some way, then the ECAV might no longer slide freely; in fact, a feasible trajectory might not exist. This idea can also be expressed using the concept of degree(s) of freedom (DOF). Any general phantom track in the x-y plane has two DOF, which can be represented in polar coordinates by R and θ with reference to a radar as the origin. Likewise, two DOF also represent any free ECAV trajectory in the same plane and can be represented by r and θ (see Fig. 2). Thus, an ECAV trying to generate a given phantom track will have one constraint θ, and one DOF, which is constrained once any other ECAV variable of motion is fixed.

Main-lobe, as opposed to side-lobe, technique deception has the primary advantage in that it is less sophisticated to execute. Its main disadvantage is the ability of producing only one phantom

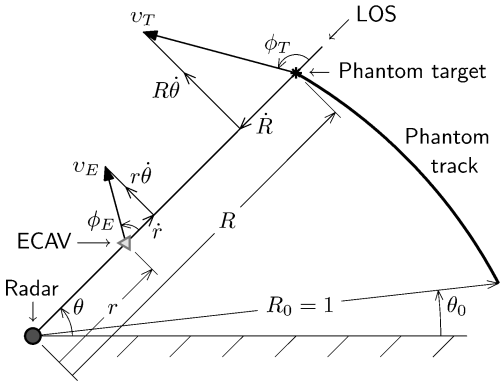

Fig. 2 Variables and relations for an ECAV engaged in main-lobe technique deception and creating a generic phantom track.

track when the number of ECAVs equals the number of networked radars. Challenges for main-lobe deception include 1) inaccuracy of ECAV and especially radar positions—an estimation problem; 2) limitations on ECAV dynamics as a result of bounded ranges for its speed, antennas, and the phantom target speed; 3) minimizing the aggregate cost of an ECAV team through choosing certain parameters of the phantom track—a (desirably decentralized) cooperative control problem; 4) providing the processing and transmission power required for DRFM; and 5) meeting the electronic requirements for generating radar pulse returns with sufficiently accurate range and Doppler frequency information. The first item listed is the subject of ongoing research[11] but is not discussed herein. The second and third items are addressed by the bulk of this paper. The fourth and fifth items would require advanced and perhaps confidential knowledge on radar and EW.

III. Results of a Constant-Speed ECAV and Phantom Track

Understanding first the dynamic limitations imposed on an ECAV when its speed and the phantom track speed are assumed constant motivates the later relaxation to bounded ranges for these speeds. Using main-lobe technique deception as just explained and with the ECAV's one DOF constrained by a constant speed, the inverse problem is now solved: given a time-dependent phantom track and an ECAV's initial position, synthesize the ECAV trajectory required to create the desired phantom track. For ease of comparison, the following nondimensional variables are used, with $v_E = 1$ and $R_0 = 1$.

$$t \to (v_E/R_0)t, \qquad r \to r/R_0, \qquad \alpha \to v_T/v_E, \qquad R \to R/R_0$$

The time-dependent speed ratio α is now used to quantify the speed of the phantom target. With these definitions, Fig. 2 illustrates the appropriate variables and their relations. For the analysis in this section, a straight constant-speed phantom track is used, and $\theta_0 = 0$ is chosen.

The basic equations of motion for the ECAV in polar coordinates are as follows. Every derivative is taken with respect to time.

$$\dot{r} = \cos\phi_E, \qquad r(0) = r_0 \tag{1}$$

$$\dot{\theta} = (1/r)\sin\phi_E, \qquad \theta(0) = 0 \tag{2}$$

Without loss of generality, $\dot{\theta}$ is assumed positive. Manipulating Eqs. (1) and (2) results in the following differential equations, which describe how r changes with time based on 1) the ECAV's constant speed of one and 2) $\dot{\theta}(t)$ of the phantom track. Of course, only one of the two equations can be used at a given time.

$$\dot{r} = \sqrt{1 - (r\dot{\theta})^2}, \qquad r(0) = r_0 \tag{3}$$

$$\dot{r} = -\sqrt{1 - (r\dot{\theta})^2}, \qquad r(0) = r_0 \tag{4}$$

For both equations, the ECAV's range must satisfy the following inequality for a solution to exist; if $\dot{\theta}$ were not assumed positive, its absolute value would be taken in this inequality:

$$r(t) < [1/\dot{\theta}(t)] \quad \forall t \tag{5}$$

If condition (5) is not satisfied, the solutions to Eqs. (3) and (4) become imaginary. Physically, condition (5) makes it clear that an ECAV cannot fly at a constant speed of one when its range is such that $r\dot{\theta}$ is greater than one (see Fig. 2). If $r\dot{\theta}$ is less than one, then the ECAV can fly at a constant speed of one by maintaining the correct $\dot{r}$ component via Eqs. (3) or (4). If either Eq. (3) or (4) reaches zero in finite time at say t_s, the condition for switching from one equation to the other at t_s is as follows, presuming $\ddot{\theta}$ is continuous (see Refs. 7 and 8 for a more complete analysis of switching).

$$\ddot{\theta}(t_s) = 0 \tag{6}$$

The parametric equations defining a straight constant-speed phantom track in polar coordinates are as follows, along with an explicit solution for $\dot{\theta}(t)$ (see Ref. 7 for a detailed development of these equations):

$$R(t) = \sqrt{1 + \alpha^2 t^2 - 2\alpha t\cos\psi} \tag{7}$$

$$\theta(t) = \arccos\left[\frac{1 - \alpha t\cos\psi}{R(t)}\right] \tag{8}$$

$$\dot{\theta}(t) = \frac{\alpha\sin\psi}{1 + \alpha^2 t^2 - 2\alpha t\cos\psi} \tag{9}$$

To solve for an ECAV trajectory given this phantom track, Eq. (9) is inserted into Eq. (3) or (4), and the solution $r(t)$ is plotted vs $\theta(t)$, which is obtained from Eqs. (7) and (8).

Figure 3 effectively explores Eqs. (3) and (4) through representative ECAV trajectory simulations for a constant-speed phantom track; the MATLAB® function ode45 was used to solve the equations with relative and absolute tolerances of 10^{-6} on the error. For each equation, the minimum and maximum initial conditions yielding a flyable ECAV trajectory for a full 90 deg of θ are shown; in this section, a flyable/feasible ECAV trajectory is one that does not reach the radar or cross the boundary represented by condition (5), which is plotted as a dash-dot line. As seen in Figs. 3a and 3c, the minimum r_0 values correspond to ECAV trajectories that start from or finish at the radar. In Figs. 3b and 3d, the maximum r_0 values correspond to trajectories that reach the $r\dot{\theta}$ boundary at $\theta = 45$ deg, satisfy condition (6), and switch from solving Eq. (3) to (4) or (4) to (3).

From observing Fig. 3, the set of feasible initial conditions for a full 90 deg of θ, [0, 0.1136] ∪ [0.4290, 1/2], is only a small subset of [0, 0.707], which contains all of the initial conditions allowing an

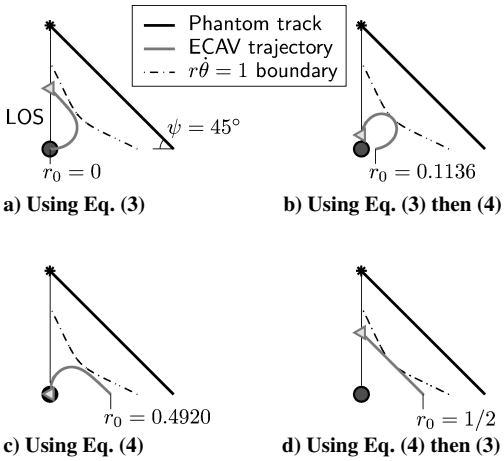

Fig. 3 Feasible constant-speed ECAV trajectory solutions for a straight constant-speed phantom track, $\alpha = 2$, $\theta \in [0, 90]$ deg.

ECAV to at least begin generating the given phantom track; furthermore, once an initial condition/starting point is chosen, the ECAV trajectory is fully constrained. These results are for no additional limitations on the ECAV such as a region of antenna operation. In conclusion, the constant-speed assumptions for the ECAV and phantom track must be relaxed to give the ECAV more flexibility in choosing its starting point and trajectory in the deception process.

IV. General Theory for ECAV Trajectory Bounds and Solutions

Because the assumption of a constant-speed ECAV and phantom track severely restricts the choice of ECAV initial conditions and trajectories, it is beneficial to make the scenario more realistic by allowing the ECAV and phantom track speeds to vary within a given range. In addition, the ECAV is now modeled as having two fixed antennas—each mounted on one side of the ECAV with less than a 90-deg look-angle from its central axis. Hence, the ECAV can no longer send pulse returns to a radar at any course angle ϕ_E.

Main-lobe technique deception is again assumed, and so the ECAV has one DOF, which will be constrained in different ways to create several ECAV dynamic systems for exploration of the ECAV's flyable range based on a given phantom track. For ease of comparison, the following nondimensional variables are used, with $v_{E\,\mathrm{m}} = 1$ and $R_0 = 1$.

$$t \to (v_{E\,\mathrm{m}}/R_0)t \qquad r \to r/R_0 \qquad a \to a/R_0$$

$$\alpha \to v_T/v_{E\,\mathrm{m}} \qquad R \to R/R_0 \qquad b \to b/R_0$$

$$v_E \to v_E/v_{E\,\mathrm{m}} \qquad \rho \to \rho/R_0$$

The speed of the phantom target is again quantified by α and is now allowed to vary. Range sets for v_E, α, and ϕ_E are written next in general form, where the minimum and maximum limits must be chosen for each variable. In this study, $\phi_{E\max} = \pi - \phi_{E\min}$ is assumed, and the specific ranges used are $\pm 20\%$ of $v_{E\,\mathrm{m}}$ for v_E, $\pm 20\%$ of 2 for α, and ± 60 deg—centered about 90 deg—for ϕ_E.

$$v_E \in [v_{E\min}, v_{E\max}], \qquad \alpha \in [\alpha_{\min}, \alpha_{\max}]$$
$$\phi_E \in [\phi_{E\min}, \phi_{E\max}] \tag{10}$$

Now for a generic phantom track and the already defined nondimensional variables, the appropriate variables and their relations are shwon in Fig. 2.

The basic equations of motion for the ECAV and phantom target, in polar coordinates, are as follows. Every derivative is taken with respect to time.

$$\dot{r} = v_E \cos\phi_E, \qquad r(0) = r_0 \tag{11}$$

$$\dot{\theta} = (v_E/r)\sin\phi_E, \qquad \theta(0) = \theta_0 \tag{12}$$

$$\dot{R} = \alpha\cos\phi_T, \qquad R(0) = 1 \tag{13}$$

$$\dot{\theta} = (\alpha/r)\sin\phi_T, \qquad \theta(0) = \theta_0 \tag{14}$$

Without loss of generality, $\dot{\theta}$ is assumed positive and given by a predetermined phantom track; throughout this paper $\dot{\theta}$ is equivalent to $\dot{\theta}(t)$. Six ECAV systems or algorithms for determining feasible ECAV trajectories are now presented in Table 1. Each system can be developed from Eqs. (11) and (12) by setting one ECAV variable constant. All systems include constraints for choosing this constant and the initial conditions to satisfy the ranges in Eq. (10), ordinary differential equations (ODEs) to solve for the ECAV trajectory, and bounds resulting from Eq. (10) that must be satisfied for all $t \in [0, t_f]$. For presentation, the straightforward expressions for $v_E(t)$ and $\phi_E(t)$ in terms of r, $\dot{r}$, and $\dot{\theta}$ are suppressed. Based on the pulse-to-pulse agility assumption, the ECAV trajectory must stop if $r(t) > R(t)$.

In Table 1, system A is simply a reformulation of Eqs. (3) and (4) for a range of constant ECAV speeds. System B allows the choice of a constant ECAV course, which is actually relative to θ

Table 1 ECAV trajectory planning algorithms

System	Initial choices/constraints	System ODE	Dynamic constraints
A	$v_{E\min} \le v_{E\,\mathrm{c}} \le v_{E\max}$ $\dfrac{v_{E\,\mathrm{c}}\sin\phi_{E\min}}{\dot{\theta}_0} \le r(0) \le \dfrac{v_{E\,\mathrm{c}}}{\dot{\theta}_0}$	$\dot{r} = \begin{cases} +\sqrt{v_{E\,\mathrm{c}}^2 - (r\dot{\theta})^2} \\ -\sqrt{v_{E\,\mathrm{c}}^2 - (r\dot{\theta})^2} \end{cases}$	$\sin\phi_{E\min} \le \dfrac{r(t)\dot{\theta}}{v_{E\,\mathrm{c}}}$ $s(t) := v_{E\,\mathrm{c}}^2 - [r(t)\dot{\theta}]^2 > 0$[a]
B	$0 < \phi_{E\min} \le \phi_{E\,\mathrm{c}} \le \phi_{E\max} < \pi$ $\dfrac{v_{E\min}\sin\phi_{E\,\mathrm{c}}}{\dot{\theta}_0} \le r(0) \le \dfrac{v_{E\max}\sin\phi_{E\,\mathrm{c}}}{\dot{\theta}_0}$	$\dot{r} = r\dot{\theta}\cot\phi_{E\,\mathrm{c}}$	$v_{E\min} \le \dfrac{r(t)\dot{\theta}}{\sin\phi_{E\,\mathrm{c}}} \le v_{E\max}$
C	$\phi_{E\min} + \theta_0 \le h_{E\,\mathrm{c}} \le \phi_{E\max} + \theta_0$ $\dfrac{v_{E\min}\sin\phi_{E0}}{\dot{\theta}_0} \le r(0) \le \dfrac{v_{E\max}\sin\phi_{E0}}{\dot{\theta}_0}$	$\dot{r} = r\dot{\theta}\cot[h_{E\,\mathrm{c}} - \theta(t)]$	$v_{E\min} \le \dfrac{r(t)\dot{\theta}}{\sin\phi_E(t)} \le v_{E\max}$
D	$\dot{v}_{E\,\mathrm{c}}$ $v_{E\min} \le v_{E0} \le v_{E\max}$ $\dfrac{v_{E0}\sin\phi_{E\min}}{\dot{\theta}_0} \le r(0) \le \dfrac{v_{E0}}{\dot{\theta}_0}$ $\dot{r}(0) = \sqrt{v_{E0}^2 - [r(0)\dot{\theta}_0]^2}$	$\ddot{r} = \dfrac{-r\dot{\theta}(r\ddot{\theta} + \dot{r}\dot{\theta}) + v_E(t)\dot{v}_{E\,\mathrm{c}}}{\dot{r}}$	$v_{E\min} \le v_E(t) \le v_{E\max}$ $\sin\phi_{E\min} \le \dfrac{r(t)\dot{\theta}}{v_E(t)}$ $s(t) := \lvert\dot{r}(t)\rvert > 0$[b]
E	$\dot{h}_{E\,\mathrm{c}}$ $\phi_{E\min} \le \phi_{E0} \le \phi_{E\max}$ $\dfrac{v_{E\min}\sin\phi_{E0}}{\dot{\theta}_0} \le r(0) \le \dfrac{v_{E\max}\sin\phi_{E0}}{\dot{\theta}_0}$ $\dot{r}(0) = r(0)\dot{\theta}_0\cot\phi_{E0}$	$\ddot{r} = \dfrac{\dot{r}(r\ddot{\theta} + \dot{r}\dot{\theta}) - v_E^2(t)(\dot{h}_{E\,\mathrm{c}} - \dot{\theta})}{r\dot{\theta}}$	$v_{E\min} \le v_E(t) \le v_{E\max}$ $\sin\phi_{E\min} \le \dfrac{r(t)\dot{\theta}}{v_E(t)}$
F	$a_{E\,\mathrm{c}}$ $v_{E\min} \le v_{E0} \le v_{E\max}$ $\dfrac{v_{E0}\sin\phi_{E\min}}{\dot{\theta}_0} \le r(0) \le \dfrac{v_{E0}}{\dot{\theta}_0}$ $\dot{r}(0) = \sqrt{v_{E0}^2 - [r(0)\dot{\theta}_0]^2}$	$\ddot{r} = \begin{cases} r\dot{\theta}^2 + \sqrt{a_{E\,\mathrm{c}}^2 - (r\ddot{\theta} + 2\dot{r}\dot{\theta})^2} \\ r\dot{\theta}^2 - \sqrt{a_{E\,\mathrm{c}}^2 - (r\ddot{\theta} + 2\dot{r}\dot{\theta})^2} \end{cases}$	$v_{E\min} \le v_E(t) \le v_{E\max}$ $\sin\phi_{E\min} \le \dfrac{r(t)\dot{\theta}}{v_E(t)}$ $s(t) := a_{E\,\mathrm{c}}^2 - [r(t)\ddot{\theta} + 2\dot{r}\dot{\theta}]^2 > 0$

[a] If $s(t) = 0$ and condition (6) is satisfied, then switching to solving the other case of the ODE is valid.
[b] If $s(t) = 0$, then switching to $-\dot{v}_{E\,\mathrm{c}}$ and perturbing $\dot{r}$ across zero allows solution of the ODE to continue.

(see Fig. 2); a course of 90 deg would result in a circular trajectory. The ODE in system B can actually be solved explicitly for $r(t)$. System C allows the choice of a constant ECAV heading, which means that the ECAV will fly in a straight line with the specified heading. System D allows the choice of a constant ECAV speed rate and is not too useful because $s(t)$ quickly reaches zero for most initial conditions. System E allows the choice of a constant ECAV turn rate and is quite helpful in testing the minimum and maximum feasible r_0 values for a specified range of θ. System F allows the choice of a constant ECAV acceleration and is more useful for a circular phantom track so that an ECAV acceleration greater (less) than the track's inherent centripetal acceleration causes the ECAV to spiral in (out) with reference to the radar.

The variable definitions and ranges for ECAV speed and course in Eq. (10) give rise to the following $r\dot{\theta}$ boundaries for the ECAV, which are similar in concept to condition (5) and apply for any phantom track.

$$r(t) = \upsilon_{E\,\min}/\dot{\theta} \tag{15}$$

$$r(t) = \upsilon_{E\,\max}/\dot{\theta} \tag{16}$$

$$r(t) = \upsilon_{E\,\min}\sin\phi_{E\,\min}/\dot{\theta} \tag{17}$$

$$r(t) = \upsilon_{E\,\max}\sin\phi_{E\,\min}/\dot{\theta} \tag{18}$$

When plotted vs $\theta(t)$, Eqs. (15–18) form boundary lines having important physical meaning. If the ECAV range decreases below boundary (15), the ECAV can continue its trajectory, but not perpendicular to the current LOS because a nonzero $\dot{r}$ component is required to fly above its minimum speed. The ECAV range can not exceed boundary (16) at any time because this would require the ECAV to fly faster than its maximum speed. The ECAV range can not decrease below boundary (17) at any time because the ECAV's region of antenna operation would rotate away from the radar even at minimum speed. Finally, if the ECAV range decreases below boundary (18), the ECAV can continue its trajectory, but only at a speed sufficiently less than its maximum.

To reduce the parametric complexity caused by variation in both υ_E and α, the phantom target speed range is converted into a larger pseudorange for the ECAV speed with the intent of modifying boundaries (15–18). Using that α is inversely proportional to $\upsilon_{E\,\mathrm{m}}$ ($\upsilon_{E\,\mathrm{m}} = 1$ is momentarily suspended) and with υ_T virtually held constant to the nominal speed used in calculating the phantom track, the following pseudolimits are determined for the ECAV speed. An alternative development of these limits is given in Ref. (9) by first showing that $\dot{\theta}(\theta)$ is directly proportional to α.

$$\upsilon_{E\,\mathrm{psmin}} = (\alpha_{\mathrm{m}}/\alpha_{\max})\upsilon_{E\,\mathrm{m}}(\upsilon_{E\,\min}/\upsilon_{E\,\mathrm{m}}) = \upsilon_{E\,\min}/(\alpha_{\max}/\alpha_{\mathrm{m}}) \tag{19}$$

$$\upsilon_{E\,\mathrm{psmax}} = (\alpha_{\mathrm{m}}/\alpha_{\min})\upsilon_{E\,\mathrm{m}}(\upsilon_{E\,\max}/\upsilon_{E\,\mathrm{m}}) = \upsilon_{E\,\max}/(\alpha_{\min}/\alpha_{\mathrm{m}}) \tag{20}$$

In these equations, α_{m} should be regarded strictly as the nominal speed used in calculating the (baseline) phantom track. The idea behind Eqs. (19) and (20) is that increasing (decreasing) the phantom target speed allows the ECAV to enter regions that previously would have required it to fly slower (faster) than permitted, hence the notion of extended pseudo speed limits. To incorporate these new regions into the $r\dot{\theta}$ boundaries, $\upsilon_{E\,\mathrm{psmin}}$ and $\upsilon_{E\,\mathrm{psmax}}$ are substituted for $\upsilon_{E\,\min}$ and $\upsilon_{E\,\max}$, respectively, in Eqs. (15–18); the modified $r\dot{\theta}$ boundaries are shown next and are later used to determine ECAV flyable ranges:

$$r(t) = \frac{\upsilon_{E\,\mathrm{psmin}}}{\dot{\theta}} = \frac{\upsilon_{E\,\min}}{(\alpha_{\max}/\alpha_{\mathrm{m}})\dot{\theta}} \tag{21}$$

$$r(t) = \frac{\upsilon_{E\,\mathrm{psmax}}}{\dot{\theta}} = \frac{\upsilon_{E\,\max}}{(\alpha_{\min}/\alpha_{\mathrm{m}})\dot{\theta}} \tag{22}$$

$$r(t) = \frac{\upsilon_{E\,\mathrm{psmin}}\sin\phi_{E\,\min}}{\dot{\theta}} = \frac{\upsilon_{E\,\min}\sin\phi_{E\,\min}}{(\alpha_{\max}/\alpha_{\mathrm{m}})\dot{\theta}} \tag{23}$$

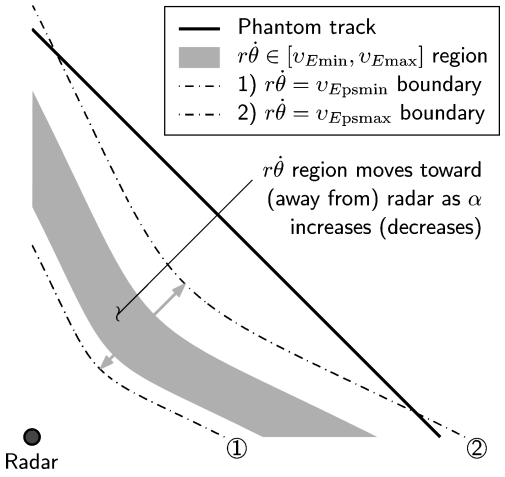

Fig. 4 Modification of $r\dot{\theta}$ boundaries based on phantom target speed range $[\alpha_{\min}, \alpha_{\max}]$.

$$r(t) = \frac{\upsilon_{E\,\mathrm{psmax}}\sin\phi_{E\,\min}}{\dot{\theta}} = \frac{\upsilon_{E\,\max}\sin\phi_{E\,\min}}{(\alpha_{\min}/\alpha_{\mathrm{m}})\dot{\theta}} \tag{24}$$

Figure 4 illustrates how $r\dot{\theta}$ boundaries (21) and (22) are created by varying α to move the $r\dot{\theta}$ region bounded by Eqs. (15) and (16) in or out to further limits. This visual explanation is similar for boundaries (23) and (24). It is important to realize that the pseudominimum ($\alpha = \alpha_{\max}$) and pseudomaximum ($\alpha = \alpha_{\min}$) boundaries cannot coexist at the same instant because α can only be one value at any given time. This fact is important primarily in the case of multiple ECAVs and multiple radars because it constrains all ECAVs to be within an area based on the $r\dot{\theta}$ region, even though over time that region can move as shown in Fig. 4. When accommodating an ECAV's desired position or speed, α will have to modulate in a continuous and believable fashion, especially if the radar is operating at a high PRF.

To aid the description of ECAV flyable ranges in subsequent sections, the following pseudo speed isolines are used, where $R(t)$ is given by the phantom track being generated:

$$r(t) = (\upsilon_{E\,\mathrm{psmin}}/\alpha_{\mathrm{m}})R(t) = (\upsilon_{E\,\min}/\alpha_{\max})R(t) \tag{25}$$

$$r(t) = (\upsilon_{E\,\mathrm{psmax}}/\alpha_{\mathrm{m}})R(t) = (\upsilon_{E\,\max}/\alpha_{\min})R(t) \tag{26}$$

For any phantom track defined by continuously differentiable functions $X(t), Y(t)$, the following three equations provide a general tool for redefining the track in polar coordinates, which is used next. If $X(t), Y(t)$ is just a profile of data points, this tool can still be used—with finite differences to approximate $\dot{X}$ and $\dot{Y}$—to convert to polar coordinates and to practically compute online the $r\dot{\theta}$ boundaries and speed isolines for an ECAV using Eqs. (21–26):

$$R(t) = \|(X, Y) - p\| \tag{27}$$

$$\theta(t) = \arg(X - p_x, Y - p_y) \tag{28}$$

$$\dot{\theta}(t) = \frac{-\dot{X}(Y - p_y) + \dot{Y}(X - p_x)}{\|(X, Y) - p\|^2} \tag{29}$$

V. ECAV Bounds for a Straight Phantom Track

The results from the preceding section involving ranges for the ECAV speed, phantom target speed, and ECAV course (region of antenna operation) are now utilized to survey the ECAV flyable range for a straight phantom track, which is described by the following parametric equations. The equations for $R(t)$ and $\dot{\theta}(t)$ can be derived from Eqs. (27) and (29) with $X(t) = 1 - \alpha t\cos\psi$, $Y(t) = \alpha t\sin\psi$, and $p = (0, 0)$.

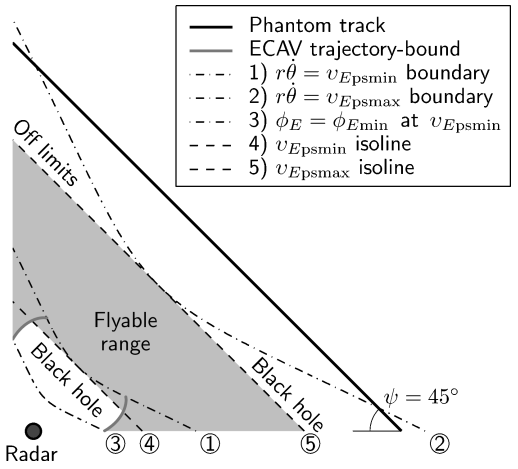

Fig. 5 ECAV flyable range for a straight phantom track, where $v_E \in [0.8, 1.2]$, $\alpha \in [1.6, 2.4]$, $\phi_E \in [30, 150]$ deg, and $\theta \in [0, 90]$ deg.

$$R(t) = \sqrt{1 + \alpha^2 t^2 - 2\alpha t \cos\psi} \tag{30}$$

$$\theta(t) = \arccos\left[\frac{1 - \alpha t \cos\psi}{R(t)}\right] + \theta_0 \tag{31}$$

$$\dot{\theta}(t) = \frac{\alpha \sin\psi}{1 + \alpha^2 t^2 - 2\alpha t \cos\psi} \tag{32}$$

Using Eqs. (30–32) with $\theta_0 = 0$, $\psi = 45$ deg, and $\alpha = \alpha_m = 2$, a straight phantom track is plotted in Fig. 5 along with the boundaries and isolines corresponding to Eqs. (21–23), (25), and (26); the boundaries and isolines account for actual variation of α within its limits in Eq. (10). The flyable range shaded in gray represents the union of all positions an ECAV could visit on certain trajectories and still be able to create the phantom track through $\theta = 90$ deg.

Many ECAV trajectories—solved using dynamic systems A–F in the preceding section—were used to test and verify the limits of the flyable range in Fig. 5. The part of the flyable range bounded by the pseudo speed isolines is valid because any trajectory parallel to and between these two isolines is within the ECAV pseudo speed range and course range. The part of the flyable range below the $v_{E\,\text{psmin}}$ isoline is actually bounded by an ECAV trajectory solved using system A with constant speed $v_{E\,\text{psmin}}$, where the ECAV is initially and finally on the inner dash-dot boundary, that is, its course is $\phi_{E\min}$ (or $\phi_{E\max}$, which corresponds to the same boundary because $\sin\phi_{E\min} = \sin\phi_{E\max}$) at $\theta = 0$ and 90 deg.

The right "black hole" in Fig. 5 is an area that can be entered by the ECAV but not exited, causing it to eventually run into the $r\dot{\theta} = v_{E\,\text{psmax}}$ boundary. To explain this mathematically, the following equation for the ECAV speed at any instant of time is used:

$$v_E = \sqrt{\dot{r}^2 + (r\dot{\theta})^2} \tag{33}$$

Suppose the ECAV is flying on the $v_{E\,\text{psmax}}$ isoline that bounds the black hole. Entering the black hole corresponds to decreasing $|\dot{r}|$, which causes v_E to decrease (from $v_{E\,\text{psmax}}$) according to Eq. (33). For the ECAV to exit, $|\dot{r}|$ would have to increase, requiring it to fly faster than $v_{E\,\text{psmax}}$ by Eq. (33). A similar argument can be used to show that the "off-limits" region can be exited by the ECAV but not entered from its flyable range. The left black hole cannot be exited and, once entered, requires that the ECAV turn in towards the radar at an increasing rate to stay within its pseudo speed range; at best, the ECAV will attain the inner dash-dot boundary but before $\theta = 90$ deg is reached.

In addition to the speed and course bounds on the flyable range for a straight phantom track, there exist ultimate θ bounds. Basically, when the angle between the phantom track and the current LOS becomes small, $\dot{\theta}$ will decrease and force the ECAV to adjust ϕ_E, in keeping with its lower speed limit, such that its region of antenna operation moves away from the radar; this will occur soon after Eqs. (23) and (24) become greater than Eqs. (25) and (26), respectively. Therefore, conservative minimum and maximum values for θ—exact when the ECAV flies parallel to the straight phantom track—can be written as follows:

$$\theta_{\min} = (\Phi - \pi/2) - (\pi/2 - \phi_{E\min}) \tag{34}$$

$$\theta_{\max} = (\Phi - \pi/2) + (\pi/2 - \phi_{E\min}) \tag{35}$$

True upper and lower bounds for θ can also be determined by equating Eqs. (23) and (26) and observing that the result does not depend on ψ. These minimum and maximum values for θ, written next, might not be achievable, but current efforts have already shown through simulation that more than 80% of the difference between these and the preceding conservative values can be reached by certain reasonable ECAV trajectories.

$$\bar{\theta}_{\min} = \Phi - \pi/2 - \arccos(v_{E\,\text{psmin}} \sin\phi_{E\min}/v_{E\,\text{psmax}}) \tag{36}$$

$$\bar{\theta}_{\max} = \Phi - \pi/2 + \arccos(v_{E\,\text{psmin}} \sin\phi_{E\min}/v_{E\,\text{psmax}}) \tag{37}$$

The analysis in this section is modular for any number of ECAVs and the same number of radars. The parameters ψ, θ_0, and R_0 are simply calculated per radar, and a separate set of phantom track equations is used for each radar/ECAV pair and flyable range so that together the ECAV team creates one coherent straight phantom track with speed α.

VI. ECAV Bounds for a General Circular Phantom Track

The results from Sec. IV are now utilized to survey the ECAV flyable range for a general circular phantom track, that is, a circular track with the radar placed arbitrarily, which is described by the following parametric equations. These equations can be derived from Eqs. (27–29) with $X(t) = \rho\cos(\alpha/\rho)t$, $Y(t) = \rho\sin(\alpha/\rho)t$, $p = (a, b)$, and $(\rho - a)^2 + b^2 = 1$:

$$R(t) = \sqrt{1 + 2a\rho - 2a\rho\cos(\alpha/\rho)t - 2b\rho\sin(\alpha/\rho)t} \tag{38}$$

$$\theta(t) = \arg[-a + \rho\cos(\alpha/\rho)t, -b + \rho\sin(\alpha/\rho)t] \tag{39}$$

$$\dot{\theta}(t) = [\alpha/R^2(t)][\rho - a\cos(\alpha/\rho)t - b\sin(\alpha/\rho)t] \tag{40}$$

where

$$\rho = a \pm \sqrt{1 - b^2}, \qquad \rho > 0$$

$$\beta = \arg(a, b)$$

Two new parameters a and b must be independently chosen to fully specify the track. Practical use of the preceding equations would entail choosing ρ independently also, instead of $R_0 = 1$ as in this study. One cumbrance of Eq. (39) is that θ_0 cannot be freely selected, or Eqs. (38–40) rely on starting the circular phantom track at a bearing of 0 deg from its center. To circumvent this problem, perform a rotational transformation on a and b based on the desired starting bearing/angle with reference to the center of the track circle, substitute the transformed a and b into the phantom track equations, and add the starting angle to $\theta(t)$ obtained from Eq. (39).

Using Eqs. (38–40) with $a = -0.38$, $b = 0.22$, and $\alpha = \alpha_m = 2$, a circular phantom track is plotted in Fig. 6 along with the boundaries and isolines corresponding to Eqs. (21–23), (25), and (26); the boundaries and isolines account for actual variation of α within its limits in Eq. (10). The flyable range shaded in gray represents the union of all positions the ECAV could visit on certain trajectories and still be able to create the full half-circle phantom track.

Many ECAV trajectories—solved using dynamic systems A and E in Sec. IV—were used to test and verify the limits of the flyable range in Fig. 6. The part of the flyable range bounded by the pseudo speed isolines is valid because any trajectory coinciding with a speed isoline between these two isolines is within the ECAV pseudo speed range and course range. The part of the flyable range below the

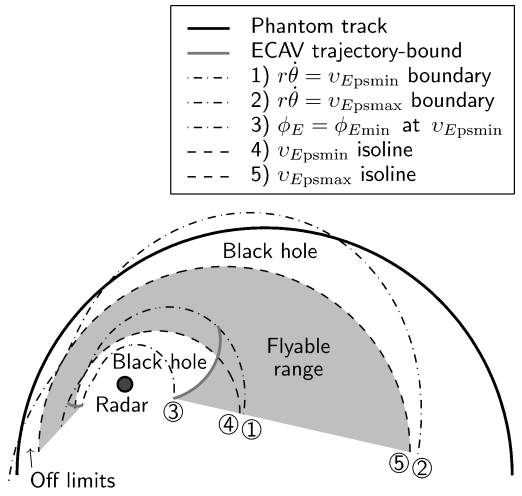

Fig. 6 ECAV flyable range for a general circular phantom track, where $v_E \in [0.8, 1.2]$, $\alpha \in [1.6, 2.4]$, $\phi_E \in [30, 150]$ deg, and $\theta \in [-13, 227]$ deg.

$v_{E\,\text{psmin}}$ isoline is actually bounded by an ECAV trajectory solved using system A with constant speed $v_{E\,\text{psmin}}$, where the ECAV is initially/finally on the inner dash-dot boundary, that is, its course is $\phi_{E\,\text{min}}$ (or $\phi_{E\,\text{max}}$, which corresponds to the same boundary because $\sin\phi_{E\,\text{min}} = \sin\phi_{E\,\text{max}}$) at $\theta = -13$ and 227 deg.

The black hole and off-limits regions in Fig. 6 are analogous to those for the straight phantom track in Fig. 5, and so their explanations are omitted here. The boundaries and isolines in Fig. 6 also appear similar to those for the straight phantom track in Fig. 5, except bent around in an elliptical shape. This observation indicates that it might be possible to determine ECAV flyable ranges for a larger class of curved phantom tracks by simply combining the results for the straight and circular tracks.

In addition to the speed and course bounds on the flyable range for a general circular phantom track, there exist ultimate θ bounds when the radar is located outside the circular track. Basically, when the angle between the phantom target's current line of direction and the current LOS becomes small, $\dot{\theta}$ will decrease and force the ECAV to adjust ϕ_E, in keeping with its lower speed limit, such that its region of antenna operation moves away from the radar; this will occur soon after Eqs. (23) and (24) become greater than Eqs. (25) and (26), respectively. Therefore, conservative minimum and maximum values for θ—exact when the ECAV flies on a speed isoline between the $v_{E\,\text{psmin}}$ and $v_{E\,\text{psmax}}$ isolines—can be written as follows and apply only if the radar is located outside the circular phantom track:

$$\theta_{\text{min}} = \pi + \beta - \arcsin\left(\frac{\rho\cos\phi_{E\,\text{min}}}{\sqrt{a^2+b^2}}\right) \tag{41}$$

$$\theta_{\text{max}} = \pi + \beta + \arcsin\left(\frac{\rho\cos\phi_{E\,\text{min}}}{\sqrt{a^2+b^2}}\right) \tag{42}$$

The analysis in this section is modular for any number of ECAVs and the same number of radars. The parameters a, b, and R_0 are simply calculated per radar, and a separate set of phantom track equations is used for each radar/ECAV pair and flyable range so that together the ECAV team creates one coherent circular phantom track with speed α. To be tactically useful, a circular phantom track would need a relatively large radius with an appreciable component of speed toward the radar.

VII. General Bounds for ECAV Flyable Ranges

Based on the ECAV flyable ranges developed for straight and circular phantom tracks in Secs. V and VI, the following equations define the range of feasible initial conditions an individual ECAV can start from to generate a straight or circular phantom track for any allowable range of θ:

$$r_{0\,\text{min}} = v_{E\,\text{psmin}}\sin\phi_{E\,\text{min}}/\dot{\theta}_0 \tag{43}$$

$$r_{0\,\text{max}} = \min(v_{E\,\text{psmax}}/\alpha_{\text{m}}, 1) \tag{44}$$

Due to the nature of $v_{E\,\text{psmin}}$ and $v_{E\,\text{psmax}}$ as defined in Eqs. (19) and (20), the feasible initial conditions of multiple ECAVs on a team are more tightly constrained because the ECAVs share a common value for the phantom target speed (see Fig. 4 and accompanying discussion in Sec. IV). Thus, Eqs. (43) and (44) are modified for n ECAVs and n radars, applicable for each ith ECAV with $i \in \{1, \ldots, n\}$. As a reminder, α_{m} should be regarded strictly as the nominal speed used in calculating the (baseline) phantom track; fixing the actual initial speed $\alpha_0 \in [\alpha_{\text{min}}, \alpha_{\text{max}}]$, get the following:

$$(r_{0\,\text{min}})_i = \frac{v_{E\,\text{min}}\sin\phi_{E\,\text{min}}}{(\alpha_0/\alpha_{\text{m}})\dot{\theta}_{0i}} \tag{45}$$

$$(r_{0\,\text{max}})_i = \min\left(\frac{v_{E\,\text{max}}}{\alpha_0}, 1\right) \tag{46}$$

Based again on the ECAV flyable ranges developed for straight and circular phantom tracks in Secs. V and VI, the following equations define the time-dependent upper and lower bounds on the flyable range of an individual ECAV generating a straight or circular phantom track for a given allowable range of θ:

$$r_{\text{min}}(t) = \min\left[(v_{E\,\text{psmin}}/\alpha_{\text{m}})R(t), r^{A,0}(t), r^{A,f}(t)\right] \tag{47}$$

$$r_{\text{max}}(t) = \min(v_{E\,\text{psmax}}/\alpha_{\text{m}}, 1)R(t) \tag{48}$$

In Eq. (47), $r^{A,0}(t)$ and $r^{A,f}(t)$ are solutions to the ODE for ECAV system A in Table 1, and both use $v_{E\,\text{psmin}}$ for their constant speed. In addition, $r^{A,0}(t)$ uses $r_{0\,\text{min}}$ for its initial value—determined from Eq. (43); and $r^{A,f}(t)$ uses $r_{\text{f}\,\text{min}}$ for its final value—determined from Eq. (43) with subscript f substituted for subscript 0. These special bounding solutions are represented graphically for specific cases in Figs. 5 and 6 as ECAV trajectory bounds. In the special case that the combined size of $[v_{E\,\text{min}}, v_{E\,\text{max}}]$ and $[\alpha_{\text{min}}, \alpha_{\text{max}}]$ is quite small, for example, less than $\pm 5\%$, the flyable range added by $r^{A,0}(t)$ and $r^{A,f}(t)$ can be lost. An important observation from Eq. (47) is that the general lower bound on an ECAV flyable range depends, through $r^{A,0}(t)$ and $r^{A,f}(t)$, on the initial and final values of time, hence θ.

Because multiple ECAVs on a team share a common profile for the phantom target speed, Eqs. (47) and (48) are modified next for n ECAVs and n radars, applicable for each ith ECAV with $i \in \{1, \ldots, n\}$; fixing the actual phantom target speed profile such that $\alpha_{\text{min}} \le \alpha(t) \le \alpha_{\text{max}}$ for each $t \in [0, t_{\text{f}}]$ and with sufficient smoothness, get the following.

$$(r_{\text{min}})_i(t) = \min\left\{[v_{E\,\text{min}}/\alpha(t)]R_i(t), r_i^{A,0}(t), r_i^{A,f}(t)\right\} \tag{49}$$

$$(r_{\text{max}})_i(t) = \min[v_{E\,\text{max}}/\alpha(t), 1]R_i(t) \tag{50}$$

In Eq. (49), $r_i^{A,0}(t)$ and $r_i{}^{A,f}(t)$ now use $v_{E\,\text{min}}/[\alpha(t)/\alpha_{\text{m}}]$ as their variable speed in solving the ODE for ECAV system A. Note that ECAV flyable ranges can be altered by choosing different profiles for $\alpha(t)$ in Eqs. (49) and (50), but $\alpha(t)$ must be the same for all n ECAVs.

VIII. Formulation of a Decentralized Cooperative Problem

A decentralized cooperative control problem—one of minimizing communication, distributing computation, coordinating trajectories, and selecting an optimal phantom track based on the ECAV team cost—is now described and its solution outlined using coordination structures[12] and the general bounds in the preceding section. The aim is to show one way these bounds can be usefully applied to control the ECAV team. The coordination function approach is not centralized; it is an implicit coordination form, which is sometimes

called redundant centralized. A coordination function describes how an individual vehicle's cost depends on the team coordination variables (the geometry and speed of the phantom track), which must be chosen the same for all vehicles. All of the coordination functions are shared among the vehicles, but there is no leader. The vehicles synchronize their databases and so arrive at the same solution because they compute the same aggregate cost function; thus, they are implicitly coordinated. An explicit coordination scheme would vote or agree on a plan (the phantom track). In general, plan negotiating schemes are not as preferable for highly coupled tasks such as generating a phantom track.

This problem is illustrated for a team of n ECAVs using main-lobe technique deception on n radars by generating a straight phantom track. To begin, assume that the track will have heading Φ and that limits for v_E, α, and ϕ_E have already been given as in Eq. (10), then mathematically define the following with $i \in \{1, \ldots, n\}$; observe that $\mathcal{T}_B$ depends on all p_i, all $(R_{\max})_i$, $\phi_{E\min}$ and $\phi_{E\max}$, and Φ.

$$p_i = (p_{xi}, p_{yi}) \in \mathbb{R}^2$$

$$D_i = \left\{ q \in \mathbb{R}^2 \mid \|q - p_i\| \le (R_{\max})_i \right\}$$

$$C_i = \left\{ q \in \mathbb{R}^2 \mid \Phi - \phi_{E\max} \le \arg(q_x - p_{xi}, q_y - p_{yi}) \le \Phi - \phi_{E\min} \right\}$$

$$B = \left(\cap_{i=1}^{n} D_i \right) \cap \left(\cap_{i=1}^{n} C_i \right)$$

$$\mathcal{T}_B = \{ f(x) \mid f'(x) \equiv \tan\Phi \quad \forall x \in \mathbb{R} \quad \text{and} \quad (x, f(x)) \in B \quad \text{for some} \quad x \}$$

Figure 7 illustrates the mathematics introduced so far, with $n = 3$. The horizontal lines in the space B represent functions $f(x)$ in $\mathcal{T}_B$ and are all possible candidates for the team-optimal phantom track; in other words, each can be generated given the three-radar situation and taking into account each radar's maximum range through D_i and the ultimate θ bounds in Eqs. (34) and (35), imposed by the ECAV course/antenna limits, through C_i.

Three variables have yet to be chosen before a phantom track with nominal speed is determined for the ECAV team. One approach to choosing these variables is as follows:

1) $f(x)$: Let the phantom track as a function of x be the coordination variable that is determined by decentralized cooperative optimization.

2) x_0: For simplicity, assume that the longest length of phantom track is desirable, and so choose x_0 by using the appropriate boundary of B.

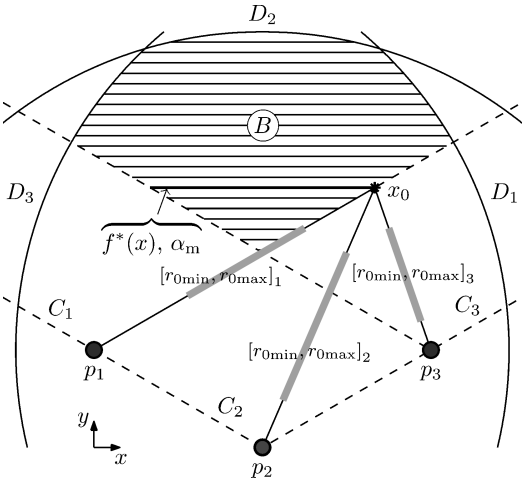

Fig. 7 Decentralized cooperative optimization scenario for $n = 3$ radars and a straight phantom track, where $\Phi = 180$ deg, $v_E \in [0.8, 1.2]$, $\alpha \in [1.6, 2.4]$, and $\phi_E \in [30, 150]$ deg.

3) α_m: Because the phantom target speed already has some allowable variation, assume that its nominal value α_m is fixed by the type of phantom target being created, but ensure $\alpha_m > v_{E\,\text{psmax}}$ to capitalize on the full ranges for v_E and α.

Given $f(x)$, x_0, and α_m, the function shown next can be defined, which uses these variables and the radar locations to solve Eqs. (45), (46), (49), and (50) with $\alpha(t) \equiv \alpha_m$ for each ECAV.

$$g[p_i, f(x), x_0, \alpha_m] \to \begin{matrix} [r_{0\min}, r_{0\max}]_i \\ [r_{\min}(t), r_{\max}(t)]_i \end{matrix}$$

The intermediate calculations needed in using Eqs. (45) and (46) to find $r_{0\min}$ and $r_{0\max}$ for each ECAV are given next, where $\alpha_0 = \alpha_m$; nondimensional variables as defined in Sec. IV are still used, but R_0 must now be calculated for each radar.

$$R_{0i} = \|(x_0, f(x_0)) - p_i\|, \qquad \theta_{0i} = \arg[x_0 - p_{xi}, f(x_0) - p_{yi}]$$

$$\psi_i = \pi - \Phi + \theta_{0i}, \qquad \dot{\theta}_{0i} = \alpha_0 \sin\psi_i$$

The additional intermediate calculations needed in using Eqs. (49) and (50) to find $r_{\min}(t)$ and $r_{\max}(t)$ for each ECAV are given next, where $\alpha = \alpha_m$:

$$R_i(t) = \sqrt{1 + \alpha^2 t^2 - 2\alpha t \cos\psi_i}$$

$$\theta_i(t) = \arccos\left[\frac{1 - \alpha t \cos\psi_i}{R_i(t)} \right] + \theta_{0i}$$

$$\dot{\theta}_i(t) = \frac{\alpha \sin\psi_i}{1 + \alpha^2 t^2 - 2\alpha t \cos\psi_i}$$

Two costs are now defined for each ECAV, where the cost functions could be based on a variety of factors such as probability of the ECAV being detected, fuel consumption, trajectory curvature, or radiated power required for deception.

$$icost_i = J_{0i}([r_{0\min}, r_{0\max}]_i, \theta_{0i})$$

$$tcost_i(t) = J_i([r_{\min}(t), r_{\max}(t)]_i, \theta_i(t))$$

For each ECAV, $icost$ quantifies how hard it would be for that ECAV to move from its current position to the initial position required for commencing a given phantom track $f(x)$. Likewise, $tcost$ quantifies the ECAV cost in flying and generating that track over time. Note that $tcost$ as defined does not depend on the positions of other ECAVs because $\alpha(t) \equiv \alpha_m$ was used for simplification.

Finally, a cost based roughly on the initial conditions and flyable ranges of each ECAV can be computed as a function of the track choice $f(x)$, which leads to the following coordination function per ECAV:

$$h_i[f(x)] \to \begin{cases} icost_i \\ tcost_i(t) \end{cases}$$

To the rest of its team, each ECAV passes a coordination function h, which gives its $icost$ or $tcost$ value for each $f(x)$ possible. Each ECAV then uses all n coordination functions and an identical routine to find $f^*(x)$ that minimizes the aggregate team cost

$$\sum_{i=1}^{n} h_i[f(x)]$$

and gives a team-optimal phantom track for the ECAVs to generate. To construct a coordination function, each ECAV must know B, Φ, and α_m.

Figure 7 illustrates the situation once the variables x_0 and α_m as well as $f^*(x)$ are chosen. The bold horizontal line represents the phantom track chosen optimally via the coordination functions, and the thick gray lines represent the ranges of initial conditions used in calculating ECAV costs. Of course, once the ECAVs choose a phantom track and begin planning their own trajectories, each ECAV will have to calculate its feasible range of initial conditions and dynamic flyable range using Eqs. (45), (46), (49), and (50), which now depend

on the team's adjustment of $\alpha(t)$ within limits. Thus, the ECAVs will have to solve a second optimization problem to again minimize their collective costs using $\alpha(t)$ as the new coordination variable.

IX. Conclusions

For main-lobe technique deception, assuming the ECAV and phantom track speeds to be constant severely limits the ECAV in terms of its feasible initial conditions and trajectories for $\theta = 0$ to 90 deg. Assuming ranges for the ECAV and phantom track speeds and accounting for the ECAV having fixed antennas with limited look angles yields a more realistic and practical flyable range for the ECAV. Flyable ranges with the preceding assumptions were thoroughly investigated, determined, and then verified via extensive ODE simulations for a straight phantom track and a general circular phantom track with radar placed arbitrarily. The theory constructed and used for this analysis may be applicable to any phantom track with sufficiently smooth geometry. The approach used to compute ECAV bounds and trajectories given a straight or circular phantom track is modular for n radars and n ECAVs.

The general bounds developed (excluding θ bounds) that define ECAV feasible initial conditions and flyable ranges are independent of the phantom track's straight or circular shape and may be applicable to other classes of curved phantom tracks. Pursuing similar results for elliptical and spiral phantom tracks would help verify this hypothesis. In the decentralized cooperative strategy presented, communicating one coordination function per ECAV—its individual cost for generating different phantom tracks—allowed the ECAV team to determine an optimal phantom track based on their aggregate bounds-dependent cost. In addition, the herein discussed deception concept provides a concrete example for the application and testing of future cooperative control algorithms.

References

[1]"Tactics, Techniques, and Procedures for Electronic Attack," U.S. Army Field Manual FM 34-45, Headquarters, Dept. of the Army, Washington, DC, June 2000.

[2]Frater, M. R., and Ryan, M., *Electronic Warfare for the Digitized Battlefield*, Artech House, Norwood, MA, 2001.

[3]"Unmanned Aerial Vehicles Roadmap 2002–2027," Office of the Secretary, U.S. Dept. of Defense, Accession No. ADA414908, Dec. 2002.

[4]Schleher, D. C., *Introduction to Electronic Warfare*, Artech House, Norwood, MA, 1986, Chap. 3.

[5]Stimson, G. W., *Introduction to Airborne Radar*, 2nd ed., SciTech Publishing, Raleigh, NC, 1998.

[6]Vakin, S. A., Shustov, L. N., and Dunwell, R. H., *Fundamentals of Electronic Warfare*, Artech House, Norwood, MA, 2001.

[7]Pachter, M., Chandler, P. R., Purvis, K. B., Waun, S. D., and Larson, R. A., "Multiple Radar Phantom Tracks from Cooperating Vehicles Using Range-Delay Deception," *Theory and Algorithms for Cooperative Systems*, edited by D. Grundel, R. Murphey, and P. M. Pardalos, World Scientific, River Edge, NJ, 2004, pp. 367–390.

[8]Pachter, M., Chandler, P. R., Larson, R. A., and Purvis, K. B., "Concepts for Generating Coherent Radar Phantom Tracks Using Cooperating Vehicles," AIAA Paper 2004-5334, Aug. 2004.

[9]Purvis, K. B., Chandler, P. R., and Pachter, M., "Feasible Flight Paths for Cooperative Generation of a Phantom Radar Track," AIAA Paper 2004-5335, Aug. 2004.

[10]Chandler, P. R., "Cooperative Control of a Team of UAVs for Tactical Missions," AIAA Paper 2004-6215, Sept. 2004.

[11]Purvis, K. B., Åström, K. J., and Khammash, M., "Estimating Radar Positions Using Cooperative Unmanned Air Vehicle Teams," *Proceedings of the American Control Conference*, Vol. 5, IEEE Publications, Piscataway, NJ, 2005, pp. 3512–3517.

[12]McLain, T. W., Chandler, P. R., and Pachter, M., "A Decomposition Strategy for Optimal Coordination of Unmanned Air Vehicles," *Proceedings of the American Control Conference*, Vol. 1, IEEE Publications, Piscataway, NJ, 2000, pp. 369–373.